Title
Thermochromic Behavior of Polydiacetylene Nanomaterials Driven by Charged Peptide Amphiphiles.

Journal
Biomacromolecules, 24(9)

Authors
Ardoña, Herdeline
Lim, Sujeung
Cordova, Dmitri
et al.

Publication Date
2023-09-11

DOI
10.1021/acs.biomac.3c00422

Peer reviewed

Biomacromolecules

Open Access

pubs.acs.org/Biomac

Article

Thermochromic Behavior of Polydiacetylene Nanomaterials Driven by Charged Peptide Amphiphiles

Published as part of the Biomacromolecules virtual special issue "Peptide Materials".

Sujeung Lim, Dmitri Leo M. Cordova, Alicia S. Robang, Yuyao Kuang, Kaleolani S. Ogura, Anant K. Paravastu, Maxx Q. Arguilla, and Herdeline Ann M. Ardoña*

Cite This: *Biomacromolecules* 2023, 24, 4051−4063

Read Online

ACCESS | Metrics & More | Article Recommendations | Supporting Information

ABSTRACT: The tunability of chromatic phases adapted by chromogenic polymers such as polydiacetylene (PDA) is key to their utility for robust sensing applications. Here, we investigated the influence of charged peptide interactions on the structure-dependent thermochromicity of amphiphilic PDAs. Solid-state NMR and circular dichroism analyses show that our oppositely charged peptide-PDA samples have distinct degrees of structural order, with the coassembled sample being in between the β-sheet-like positive peptide-PDA and the relatively disordered negative peptide-PDA. All solutions exhibit thermochromicity between 20 and 80 °C, whereby the hysteresis of the blue, planar phase is much larger than that of the red, twisted phase. Resonance Raman spectroscopy of films demonstrates that only coassemblies with electrostatic complementarity stabilize coexisting blue and red PDA phases. This work reveals the nature of the structural changes responsible for the thermally responsive chromatic transitions of biomolecule-functionalized polymeric materials and how this process can be directed by sequence-dictated electrostatic interactions.

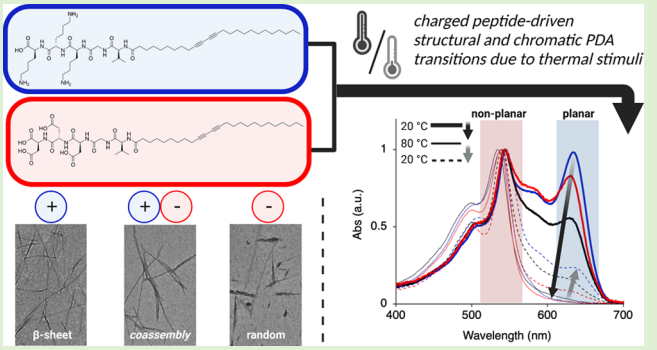

INTRODUCTION

Over the years, stimuli-responsive polydiacetylene (PDA)-based materials have been used in different sensing technologies, such as for food quality indicators,[1] for harmful substances (for the environment and humans) detectors,[2−4] and for temperature sensing.[5,6] The chromogenic properties of PDA responsible for its sensing capabilities are known to be caused by the conformational changes that this polymer affords in response to environmental stimuli such as heat.[7−9] Early reports attribute the thermochromism in PDAs to chromatic phase transitions that involve an initial planar, non-fluorescent, blue PDA phase (maximum absorption peak wavelength, λ_{max} ~630 nm) that interconverts with a fluorescent, red PDA phase (λ_{max} ~540 nm) that has a more twisted ene-yne conjugated backbone.[10−13] While this blue-to-red phase transition is more commonly observed, other chromatic states such as the yellow phase (λ_{max} ~470 nm)[14,15] or an intermediate, purple phase (λ_{max} ~590 nm) exist due to the possibility of more than two electronic structures of PDA chains, as previously reported.[13]

Similar to other functional polymers, side-chain engineering can be used to control both the topochemical polymerization of diacetylenes (DAs) and the resulting phases that PDA adapts in response to external stimuli.[12,16−20] The pathways for structural changes that are responsible for thermochromicity and their corresponding reversibility can be impacted by non-covalent interactions between side chains, such as through H-bonding interactions.[13] For instance, PDAs appended with bisurea and oligoethylene oxide moieties have been demonstrated to show a multistep color transition, involving reversible thermochromism with the blue-to-red and yellow-to-red transition.[21] On the other hand, irreversible chromatic transitions have been observed in PDA-based materials with ethylene, diethylene, and triethylene glycol methyl ethers due to the lack of adequate H-bonding interactions between ester groups within the PDA system.[22] Several of these systems utilize H-bonding moieties to process these adaptive polymers in organic solvents, but more recent examples include the use of tunable bioinspired H-bonding side groups such as peptides to demonstrate thermochromism. For example, a β-sheet-forming pentapeptide consisting of an alternating leucine (L)-lysine (K) sequence was conjugated to the DA monomers and, its polymeric form was reported to

Received: April 25, 2023
Revised: July 18, 2023
Published: August 8, 2023

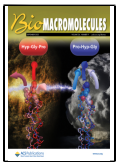

https://doi.org/10.1021/acs.biomac.3c00422
Biomacromolecules 2023, 24, 4051−4063

exhibit reversible thermochromic transitions from 10 to 68 °C.[23] Similarly, a reversible thermochromic transition from 5 to 95 °C was observed in another PDA system appended with a β-sheet-forming peptide, Lys-Thr-Thr-Lys-Ser (KTTKS).[24] A PDA system conjugated with the GAGAGAGY sequence exhibited faster and more reversible thermochromism compared to the PDA system without the peptides.[25] Altogether, these previous reports confirm that peptides can serve as templating moieties to the DA monomers that are capable of influencing the thermochromic behavior of PDAs.[23−25] However, there is still a standing knowledge gap in identifying the specific contributions of the non-covalent peptidic interactions in precisely driving the chromatic phases adapted by PDAs.

In this study, we investigate how the nature of charged interactions, coexisting with other non-covalent peptide interactions, can influence the conformational states responsible for the thermochromism of water-processable peptide-PDAs. We designed two oppositely charged peptide-DA monomers: a positively charged KKKGV (K_3GV) and a negatively charged DDDGV (D_3GV) appended to 10,12-pentacosadiynoic acid (PCDA) and used these as model monomers to probe how charged peptide-templating groups can direct interactions between DAs during their topochemical polymerization, therefore modulating their dynamic responses to thermal stimuli. By characterizing the order imparted by peptides to the overall system and monitoring the photophysical properties of these peptide-polymer conjugates in solution and film, we show how attractive/repulsive electrostatic interactions (along with H-bonding) impact the thermochromic behavior of PDAs originating from their conformational changes as mapped out in this work. Understanding how electrostatic interactions, in concert with other non-covalent peptidic interactions, cooperatively impact the parameters for the mild coassembly conditions (i.e., under neutral, aqueous conditions) of the peptide-conjugated PDA coassembly system and their resulting stimuli-responsive behavior would help in better designing future water-processable conjugated polymers as functional biomaterials endowed with tunable dynamic properties.

MATERIALS AND METHODS

General Considerations. The chemicals used for 9-fluorenylmethoxycarbonyl (Fmoc)-based solid-phase peptide synthesis (SSPS) (*N*-methylpyrrolidinone (NMP), *O*-(benzotriazole-1-yl)-*N*,*N*,*N*′,*N*′-tetramethyluronium hexafluorophosphate (HBTU), benzotriazol-1-yl-oxytripyrrolidinophosphonium hexafluorophosphate (PyBOP), trifluoroacetic acid (TFA), triisopropylsilane (TIPS), *N*,*N*-diisopropylethylamine (DIPEA), Wang resin, and Fmoc-protected amino acids) were obtained from Oakwood Products, Inc. or Advanced ChemTech. Formic acid and 10,12-PCDA were obtained from Sigma-Aldrich. *N*,*N*-Dimethylformamide (DMF), ammonium hydroxide, potassium hydroxide (KOH), and acetonitrile, methanol, dichloromethane (DCM) were obtained from Fisher Scientific. DIPEA was degassed by sparging with nitrogen (N_2) gas over 4 Å molecular sieves for 1 h prior to use. For peptide-DA coassembly polymerization, upon mixing the two components, the solution was instantaneously UV-irradiated (6-Watt, 254 nm source) for 5 min in a similar way as the neat samples. Characterization of monomer and polymer samples can be found in the Supporting Information (Figures S1−12 and Table S1).

General Solid-Phase Peptide Synthesis. Peptide segments, K_3GV and D_3GV, were synthesized via the standard Fmoc solid-phase technique either manually or with the aid of a Liberty Blue Automated Microwave Peptide Synthesizer (CEM Corporation). The Wang resins used were pre-loaded with amino acids (Wang-Asp (OtBu) = 0.32 mmol/g and Wang-Lys (Boc) = 0.65 mmol/g). To the resin in a peptide chamber, Fmoc-deprotection was done by adding a (1:4) piperidine/DMF solution twice (2- and 10 min treatments) and then washed with NMP, methanol, and DCM (3 times each). For the amino acid couplings, 3 equiv of the Fmoc-protected amino acid (relative to the resin) was activated with 2.9 equiv of HBTU and 10 equiv of DIPEA, and the mixture was mixed for 1 min prior to addition to the chamber. The chamber was mixed for 60−75 min and then washed with NMP, methanol, and DCM (3 times each). The completion of all couplings was monitored using a Kaiser test on a few dry resin beads, repeating the same amino acid coupling as needed. The general procedure was repeated until the desired peptide sequence was obtained.

10,12-PCDA Coupling. The coupling of PCDA to the peptide was done following the same procedure described previously.[26] Both peptides (C- to N-terminus: K_3GV and D_3GV) were washed with NMP, methanol, and DCM (3 times each). To the resin in a peptide chamber, Fmoc-deprotection was done by adding a (1:4) piperidine/DMF solution twice (2- and 10 min treatments) and then washed with NMP, methanol, and DCM (3 times each). 0.6 equiv of 10,12-PCDA and 0.6 equiv of PyBOP were dissolved in 10 mL of 2:1 NMP/DCM, and then 0.174 mL of DIPEA (10 equiv) was added and sonicated for 5 min. The solution was then added to Wang-K_3GV-NH_2, and the same steps were done for Wang-D_3GV-NH_2. The reaction was mixed for 12−18 h. Then, the resin was rinsed with NMP, methanol, and DCM (3 times each). The resin was subjected to the second round of coupling with 0.4 equiv of 10,12-PCDA and 0.4 equiv of PyBOP dissolved in 10 mL of 2:1 NMP/DCM with 0.174 mL of DIPEA (10 equiv). The solution was added to the chamber, and the reaction was mixed for 12−18 h. The resin was washed with NMP, methanol, and DCM (3 times each) and stored in the fridge for cleavage.

Pentacosanoic Acid Coupling. Similar to 10,12-PCDA coupling, pentacosanoic acid (PA) coupling was done following a standard amidation protocol to the peptide backbone. Wang-D_3GV-Fmoc peptide was washed with NMP, methanol, and DCM (3 times each). To the resin in a peptide chamber, Fmoc-deprotection was done by adding a (1:4) piperidine/DMF solution twice (2- and 10 min treatments) and then washing with NMP, methanol, and DCM (3 times each). 0.6 equiv of PA and 0.6 equiv of PyBOP were dissolved in 10 mL of 2:1 NMP/DCM, and then 0.174 mL of DIPEA (10 equiv) was added and sonicated for 5 min. The solution was then added to Wang-D_3GV-NH_2. The reaction was mixed for 12−18 h. Then the resin was rinsed with NMP, methanol, and DCM (3 times each). The resin was subjected to the second round of coupling with 0.4 equiv of PA and 0.4 equiv of PyBOP dissolved in 10 mL of 2:1 NMP/DCM and 0.174 mL of DIPEA (10 equiv). The solution was added to the chamber, and the reaction was mixed for 12−18 h. The resin was washed with NMP, methanol, and DCM (3 times each) and stored in the fridge for cleavage.

General Acid Cleavage. The cleavage cocktail was prepared with 9.5 mL of TFA, 250 μL of Milli-Q water, and 250 μL of TIPS. 10 mL of cleavage cocktail was added to a peptide chamber that contains the resin. Then, the same chamber was shaken using a vertical orbital shaker for 2−3 h. The filtrate was collected, and the resin was washed with DCM twice to ensure that the product was completely recovered. The filtrate was concentrated under reduced pressure, and the crude peptide-PCDA was precipitated out of the filtrate by adding ∼25 mL of cold ethyl ether. The pellet was isolated by centrifugation (10 min, 3000 rpm), followed by decanting the solvent. The pellet was redissolved in Milli-Q water. A few drops of ammonium hydroxide were added for D_3GV-PCDA to fully dissolve the pellet and was then lyophilized. For K_3GV-PCDA, only Milli-Q water was used to dissolve. Both D_3GV-PCDA and K_3GV-PCDA (crude and purified) were stored as lyophilized solids at 4 °C.

Purification Procedure. Samples were purified using reverse-phase high-performance liquid chromatography (HPLC). The HPLC sample for K_3GV-PCDA was prepared from lyophilized peptide-PCDA solids after the synthesis and was dissolved in 0.1% formic acid in Milli-Q water (pH 2−3). The HPLC sample for D_3GV-PCDA was prepared from lyophilized peptide-PCDA powder and was dissolved in 0.1% ammonium formate in Milli-Q water (pH 8−9). The mobile phase used consists of a 0.1% ammonium formate aqueous buffer (pH 8−9; for

https://doi.org/10.1021/acs.biomac.3c00422
Biomacromolecules 2023, 24, 4051−4063

D_3GV-PCDA) or 0.1% formic acid in Milli-Q water (pH 2−3; for K_3GV-PCDA) and acetonitrile. The purification was performed using an Agilent Infinity II Preparative HPLC system (column: Zorbax Eclipse XDB-C8, 21.2 × 250 mm). The purity was monitored at 220 nm by analytical HPLC (column: Zorbax 300SB-C3, 4.6 × 150 mm).

Electrospray Ionization Mass Spectrometry. Samples for ESI-MS analyses were prepared by using Milli-Q water to make the concentration of 0.1 mg/mL. Mass spectra were collected using a Waters Acquity ultra-performance liquid chromatography H-Class system in negative mode.

Nuclear Magnetic Resonance Spectroscopy. To characterize the purified peptide-DA monomers and the polymerized samples, corresponding solutions were prepared by adding 500 μL of deuterated water (D_2O) to the lyophilized samples. ^{1}H NMR spectra of the samples were recorded on GN 500 MHz (Bruker Avance), and the data were processed using MestReNova.

For the solid-state NMR (ssNMR) characterization, approximately 10 mol of peptide-DA samples (K_3GV-DA, D_3GV-DA, and 1:1 K_3GV-DA/D_3GV-DA) were prepared by dissolving lyophilized peptides in Milli-Q water at 2 mg/mL stock solutions before diluting to 10 mL. Peptide solutions were then irradiated with a 6-Watt 254 nm UV lamp to produce peptide-PDA samples. After preparation, samples were centrifuged directly into 3.2 mm NMR rotors at 280,000g at 4 °C for at least 30 min on a Beckman Optima XPN-100 with a SW-41 Ti swinging-bucket rotor. The NMR rotors were placed in a custom-made polycarbonate funnel widget fitted into 13.2 mL Ultra-Clear tubes. The ^{13}C NMR spectra were collected using ^{1}H-^{13}C cross-polarization magic angle spinning (CPMAS) measurements on a 11.75 T Bruker Avance III spectrometer with 100 kHz decoupling. The MAS spinning speed was 10 kHz. Chemical shifts were referenced to tetramethylsilane after calibration with glycine before measurements. Signals were averaged over 24 h of scanning.

Gel Permeation Chromatography. A Shimadzu HPLC (UV, LC-2050) with a Wyatt Technology miniDAWN Multi-Angle Light Scattering (LS, MALS) and a Wyatt Technology differential refractometer (dRI, Optilab) was used to characterize the molecular weight and polydispersity index of peptide-polymer samples. A silica-based column [300 Å, 7.8 × 300 mm (WTC-030S5)] was used with pH 7 water as the eluent with a flow rate of 1 mL/min. The column was equilibrated using polyacrylic acid-Na salt standards.

Ultraviolet-to-Visible Absorption Spectroscopy. UV-Vis absorption spectra of the peptide-polymer conjugate samples were obtained using a Cary 100 UV-Vis spectrophotometer. Samples were prepared in the following way: 2.2 mM K_3GV-PCDA and 2.3 mM D_3GV-PCDA stock solutions were prepared with pH 7 Milli-Q water, and then pH was measured for both stock solutions. To prepare the neat samples (K_3GV-PDA and D_3GV-PDA), the samples were diluted with pH 7 Milli-Q water to have the final concentration of each sample as 0.66 mM. For the 1:1 coassembly sample, the corresponding volume of both monomers was combined and diluted with pH 7 Milli-Q water to have a final concentration of 0.66 mM. The pH of all three samples was measured again to make sure it was neutral. Then the three samples were exposed to the UV (254 nm) for 5 min, and then each sample solution was instantly polymerized. In general, a Cary Dual Cell Peltier accessory was used to control and maintain the temperature for measurements at different temperatures (20, 40, 60, and 80 °C).

To monitor the thermochromism of the peptide-PDA conjugates, samples were prepared at room temperature and then exposed to the four temperatures mentioned above. The colorimetric response (CR) was quantified from UV-vis spectra after 1 cycle of heating and cooling using the following equation: $\mathrm{CR}(\%) = \frac{(PB_i - PB_f)}{PB_i} \times 100$, where percent blue (PB) is defined as the following from a previous report:[26,27] $\mathrm{PB} = \frac{A_{blue}}{(A_{red} + A_{blue})}$. A_{blue} and A_{red} are the raw absorbance values of the aqueous peptides-PDA at $\lambda_{blue,max}$ ~630 nm and at $\lambda_{red,max}$ ~530 nm.

Circular Dichroism Spectroscopy. For both the room temperature and the variable temperature measurements, circular dichroism (CD) spectra were obtained using a Jasco J-810 spectropolarimeter. The same samples prepared and used for UV-vis spectroscopy were diluted to 0.066 mM to obtain the measurements. CD spectra were measured at 190−260 nm for the peptide. For variable temperature measurements, the Jasco PFD 425S temperature controller was used to maintain a constant temperature during each run. CD spectra were taken for each sample as temperatures varied from 20 to 80 °C with 20 °C increments.

Transmission Electron Microscopy. Images were obtained using a JEOL JEM-2100F equipped with a Gatan K3 direct electron detector and a Gatan OneView camera at an operating voltage of 80−200 kV. The samples were prepared using the same methods to prepare for UV-vis and CD. The transmission electron microscopy (TEM) grids were prepared by pipetting 5 μL of each peptide-PDA solution onto 200 mesh copper grids coated with a Formvar film (Electron Microscopy Sciences) and 4 nm carbon coating and adsorbed for 30 s at room temperature. The grid was washed with fresh Milli-Q water right away to prevent the sample from drying, and the excess solution was removed by touching the side of each grid with filter paper. The sample was then stained with a 1% uranyl acetate solution for 30 s and washed with fresh Milli-Q water, and excess moisture was removed.

Temperature-Dependent Raman Spectroscopy. The samples used for Raman spectroscopy were prepared as follows: 2.2 mM K_3GV-PCDA and 2.3 mM D_3GV-PCDA stock solutions were prepared with pH 7 Milli-Q water, and then pH was measured for both stock solutions. The neat samples (K_3GV-PDA and D_3GV-PDA) were diluted with pH 7 Milli-Q water to have the final concentration of each sample as 0.66 mM. For the 1:1 coassembled sample, the corresponding volume of both monomers was combined and diluted with pH 7 Milli-Q water to have a final concentration of 0.66 mM. The pH of all three samples was measured prior to exposing the samples to UV (254 nm) for 5 min. After 5 min, each sample solution was instantly polymerized. Thin-film samples of peptide-PDA samples were prepared by drop-casting 40 μL of the solution onto glass coverslips or SiO_2/Si substrates. A Linkam THMS600 temperature-controlled stage was used to control the sample temperature during the temperature-dependent Raman spectroscopy experiments. To ensure good thermal contact between the thermal stage and the sample, the substrates were secured to the stage using silver paste (Fast Drying Silver Paint Electrodrag 1415, Ted Pella) as an adhesive. Throughout the analysis, the samples were purged with Ar gas to ensure an inert atmosphere. At each temperature measurement point, the temperature was allowed to equilibrate for at least 5 min. Raman spectra were collected on a system based on a Renishaw inVia microscope (532 nm laser) and a Horiba LabRAM HR Raman spectrometer (473, 633, and 785 nm). The measurements were done using 473, 532, 633, and 785 nm lasers with a nominal power of 3 mW and a long working distance of 5× objective. Five temperatures (20, 40, 60, 80, and 100 °C) were chosen to be tested for variable temperature measurements. To probe the thermochromic properties, samples that were prepared at room temperature were exposed to the pre-determined temperatures stepwise while performing in situ Raman spectroscopy at each temperature point.

RGB Analysis of Film Images. Optical images of the thin films were captured using the Renishaw inVia microscope equipped with an OMAX 18.0 MP USB 3.0 Digital Camera and coupled with a 0.01 mm calibration slide at each temperature. The image analysis for all samples was done on the ImageJ software. First, the images were corrected for small lighting and exposure deviations by using white balance correction (https://github.com/pmascalchi/ImageJ_Auto-white-balance-correction). Then, the color histograms containing the distribution of RGB values for selected homogeneous regions of interest were obtained.

Attenuated Total Reflectance-Fourier Transform Infrared Spectroscopy. Stock solutions of 2.2 mM K_3GV-PCDA and 2.3 mM D_3GV-PCDA were prepared with Milli-Q water and adjusted to pH 7 using 1 M KOH as needed. The neat samples (K_3GV-DA and D_3GV-DA) were diluted with pH 7 Milli-Q water to have the final concentration of each sample as 0.66 mM. For the 1:1 coassembled sample, the corresponding volume of both monomers was combined and diluted with pH 7 Milli-Q water to have a final concentration of 0.66 mM. The pH of all three samples was measured prior to exposing

https://doi.org/10.1021/acs.biomac.3c00422
Biomacromolecules 2023, 24, 4051−4063

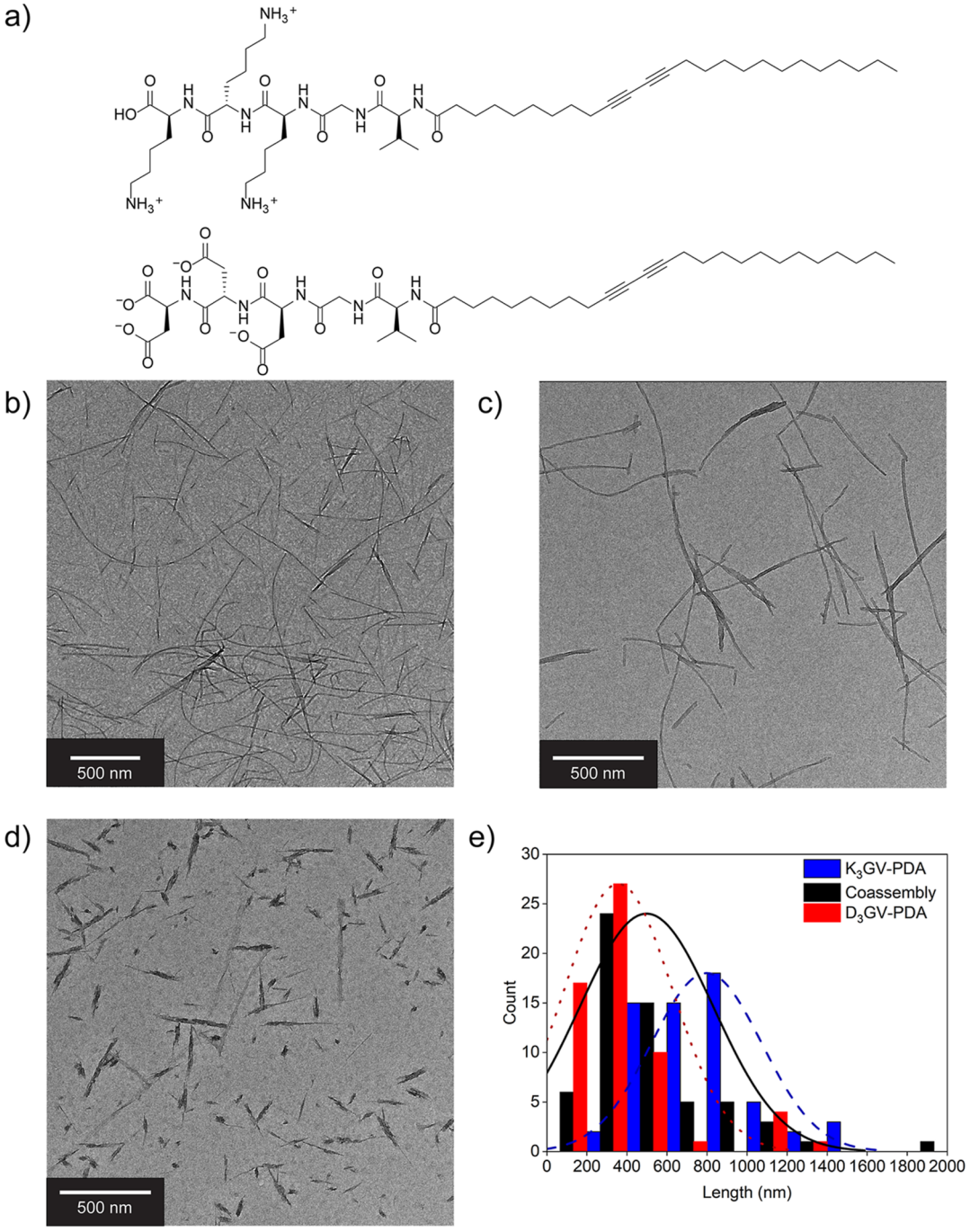

Figure 1. Molecular structures of charged peptide-DAs and its representative TEM images. (a) Chemical structures of K_3GV-DA and D_3GV-DA. Representative TEM images of assembled samples (0.66 mM concentration for each sample) at pH 7: (b) K_3GV-PDA; (c) equimolar (1:1) coassembly of K_3GV-PDA with D_3GV-PDA; and (d) D_3GV-PDA. (e) Length distribution from TEM images of the coassembly of K_3GV-PDA and D_3GV-PDA and its individual components (n = 3 images and 3 views per image). K_3GV-PDA: 798 ± 159 nm; coassembly: 498 ± 193 nm; and D_3GV-PDA: 357 ± 156 nm. Scale bar = 500 nm.

the samples to a 254 nm light sourcefor 5 min. Peptide-PDA samples were exposed to one heating-cooling cycle (20−80 °C, back to 20 °C) at a rate of 4 °C/min. After one cycle of heating-cooling, the samples were lyophilized. The Fourier-transform infrared (FTIR) spectra of solid samples were collected using a Jasco FT/IR-4700 spectrometer equipped with a single bounce attenuated total reflectance (ATR) attachment with a monolithic diamond and a triglycine sulfate detector. The FTIR spectra were measured in the 400−4000 cm^{-1} range for all samples. For each measurement, the instrument was calibrated by obtaining a background spectra, and signals of ambient CO_2/H_2O vapor were removed as well. The final spectra were ATR-corrected and baselined.

RESULTS AND DISCUSSION

Peptide-DA Design, Assembly, and Polymerization. The two charged pentapeptide-DA monomers were used as a model system to investigate the ability of charged biomolecules that are water-soluble to impact the responsiveness of PDA optical properties to thermal stimuli. In particular, we designed two pentapeptide-DAs that are oppositely charged by including

https://doi.org/10.1021/acs.biomac.3c00422
Biomacromolecules 2023, 24, 4051−4063

charged amino acids such as lysine (K) and aspartic acid (D) into the peptide sequences at the periphery of the hydrophilic end of this amphiphile (Figures 1a and S1−S9; sequences are presented from C- to N-terminus). These two amino acids with electrostatic complementarity were chosen as commonly charged pairs that have previously been reported to stabilize the formation of hierarchically ordered peptide and protein structures.[28−30] Although there is a fair amount of reports on utilizing lysine and glutamic acid electrostatic interactions to stabilize self-assembled structures,[31,32] we empirically found the self-assembly and coassembly of our specific K- and D-containing sequences to fulfill the geometric requirements for DA polymerization. Toward the N-terminus and closer to the hydrophobic part of each amphiphilic monomer, valine (V) is incorporated due to its high propensity to form a β-sheet structure,[33] while glycine (G) is used as a spacer after charged residues. The length of the peptide segment was kept to be less than that of the alkyl chain bearing DA units to maintain the impact of the hydrophobic interactions acting in synergy with the H-bonding interactions of the peptides and enable instantaneous amphiphile assembly at pH 7. We then chose to carry out the experiments with these two specific peptide sequences, K_3GV and D_3GV, which both meet the basic requirements for our studies: (i) they bear charged residues at neutral pH, (ii) they can self-assemble and polymerize at neutral pH, and (iii) the electrostatically driven coassembly can also polymerize upon UV irradiation of the two-component assemblies. Assemblies of single components and equimolar two-component solutions (here, termed as coassemblies or coassembled samples) are all formed at pH 7, followed by polymerization via exposure to a 254 nm UV light source for 5 min. Under the aqueous polymerization conditions, the resulting K_3GV-PDA is positively charged, and D_3GV-PDA is negatively charged based on the pK_a values of the respective peptide segments. The formation of assemblies and coassemblies and the polymerization of DAs were both afforded at the concentrations described below. Peptide-PDA samples were characterized by NMR and gel permeation chromatography (GPC), whereby the NMR spectra for peptide-PDA samples show peaks that are broadened compared to the peptide-DA monomers (Figures S10 and S11), and GPC confirms that all samples were polymerized within the range of $\sim 10^7$ to $\sim 10^{10}$ Da (Figure S12 and Table S1).

The resulting nanostructures from their polymerized single-component assemblies (K_3GV-PDA and D_3GV-PDA) and their coassembly were also characterized using TEM (Figure 1b−d). These three peptide-polymer samples all form one-dimensional (1-D) nanostructures but with significant differences in the aspect ratio, similar to sequence-dependent morphological variations previously reported in other self-assembling peptide systems.[34−36] D_3GV-PDA exhibited the shortest mean length for nanostructures (with the broadest distribution), while the equimolar coassemblies are more polydisperse in nanostructure lengths, with a mean length average that is skewed closer to the mean length of D_3GV-PDA assemblies (Figure 1e). Considering the electrostatic interactions that coexist with H-bonding and hydrophobic interactions for the peptide-polymers under investigation, our charged single-component peptide-PDA samples represent the control system with repulsive electrostatic interactions, while the two-component/coassembled peptide-PDA can be considered to have both repulsive (within blocks of the same peptides) and attractive (at the interface of K_3GV and D_3GV units) electrostatic interactions.

To obtain information about the structural order and structural differences between the peptide-PDA samples, peptide-PDAs were packed into ssNMR rotors using ultracentrifugation, and ^{13}C natural abundance spectra were collected using ssNMR. All three samples were initially set to ultracentrifuge for 30 min. Only K_3GV-PDA was successfully packed into the rotor after 30 min, suggesting a higher degree of assembly. D_3GV-PDA was ultracentrifuged for an additional 4 h and 30 min, and the coassembly was left to ultracentrifuge overnight to obtain sufficient samples packed into the NMR rotors for NMR measurements. CPMAS (^1H-^{13}C CPMAS) was used to collect the ^{13}C spectra. Partial spectral assignments for the peptide templates were made using the known ^{13}C chemical shift ranges for K, D, G, and V amino acids and previously reported carbon chemical shifts for PDA (Figure 2).[37,38] The full

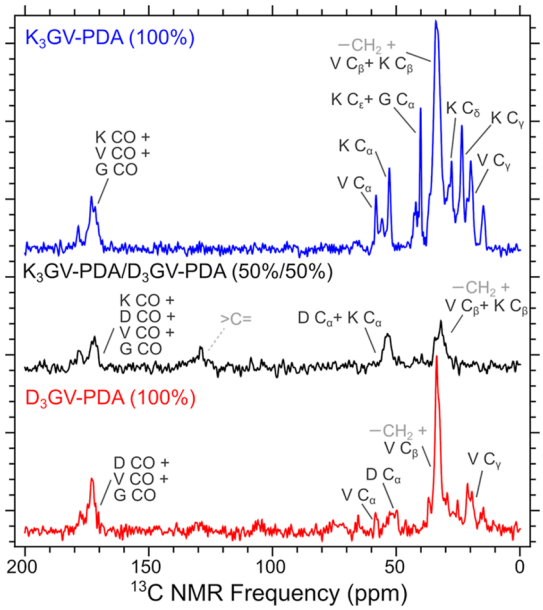

Figure 2. ^1H-^{13}C CPMAS spectrum of K_3GV-PDA, D_3GV-PDA, and coassembly of K_3GV-PDA/D_3GV-PDA. Selected peaks are labeled using known chemical shift ranges for carbons within the K, D, G, and V amino acids (text in dark gray) and PDA (text in light gray).

width at half-maximum (fwhm) of the peaks was used to evaluate the relative structural order. Narrow peak linewidths (~1 ppm) at half-maximum were observed from the data for K_3GV-PDA, indicating that K_3GV-PDA has a high structural order typical of amyloid fibrils.[39] The labeled peaks for K_3GV-PDA assign all the K, G, and V carbons within the peptide that have chemical shifts consistent with β-sheets. The high structural order of K_3GV-PDA is also consistent with observing elongated fibrils and long mean lengths from the TEM images in Figure 1.[40] Conversely, the lower peak intensity and wider peak linewidths for D_3GV-PDA show little to no assembly for D_3GV-PDA. The strongest peak observed at 32 ppm, while it has a fwhm close to one, is more consistent with the presence of $-CH_2$ within the PDA domain. The NMR data for the coassembly show peak linewidths wider than K_3GV-PDA and are closer to the disordered assembly of D_3GV-PDA. The data suggest that the addition of D_3GV-PDA to K_3GV-PDA disrupts the ordered assembly of K_3GV-PDA alone. Unlike in the single-component K_3GV-PDA and D_3GV-PDA samples, we observe a branched alkene carbon signal at approximately 130 ppm from the PDA domain in the coassembly spectrum.

https://doi.org/10.1021/acs.biomac.3c00422
Biomacromolecules 2023, 24, 4051−4063

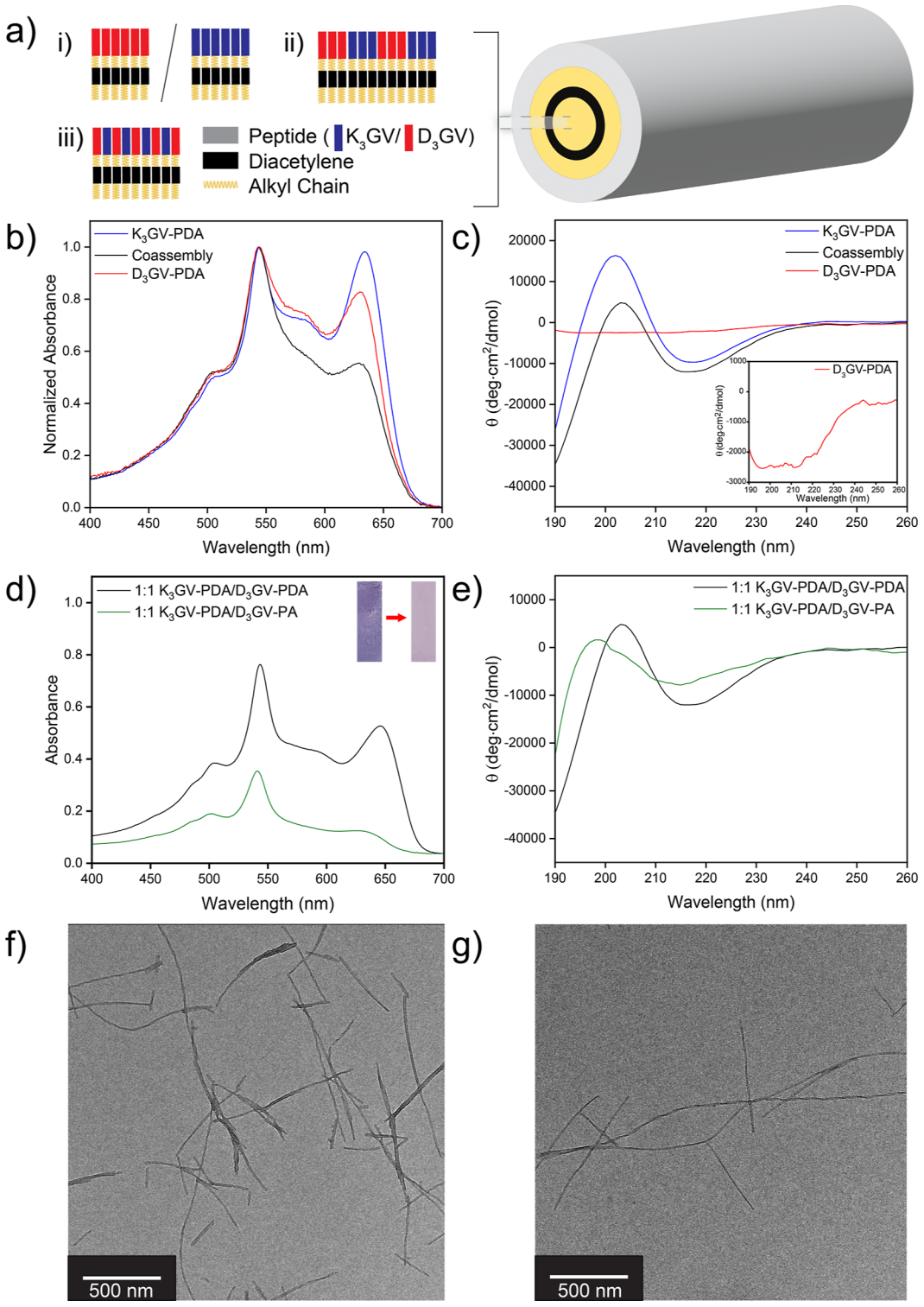

Figure 3. Photophysical and structural characterizations of the peptide-PDA system. (a) Schematic representation of the 1-D assemblies of peptide-PDAs and possible arrangements of peptide-DA assemblies: i−iii (gray: peptide moieties; blue: K_3GV; red: D_3GV; black: DA; and yellow: alkyl chains). (b) UV-vis spectra and (c) CD spectra (190−260 nm) of K_3GV-PDA, D_3GV-PDA, and coassembled samples (inset: CD spectra for D_3GV-PDA). (d) UV-vis spectra (inset: images of peptide-PDA solutions) and (e) CD spectra (190−260 nm) of K_3GV-PDA/D_3GV-PDA vs K_3GV-PDA/D_3GV-PA coassembly. Representative TEM images of (f) assembled equimolar K_3GV-PDA/D_3GV-PDA and (g) 1:1 coassembly of K_3GV-PDA with D_3GV-PA at pH 7.

The NMR results also provide us details about the coassembly formation and the relative peptide assembly tendency of the samples. For the two-component, coassembled sample, self-sorted structures are less likely to form under the assembly and polymerization conditions. If K_3GV-PDA and D_3GV-PDA did form self-sorted structures, the spectrum of the coassembly could be represented as a linear combination of the other two spectra. Because we cannot reconstruct certain signals from the

https://doi.org/10.1021/acs.biomac.3c00422
Biomacromolecules 2023, 24, 4051−4063

coassembly spectrum through the addition of the other spectra (such as the branched alkene (>C═) peak at 130 ppm), we infer that the coassembly sample produces 1-D assemblies with structural features distinct from the pure peptide-PDA samples. To estimate the peptide assembly tendency of the samples, we arbitrarily set the K_3GV-PDA peak intensity to 1 and integrated the carbonyl carbon peaks between 165 and 180 ppm. We also scaled the intensity value to the number of carbonyl carbons per peptide for comparison, assuming a 1:1 stoichiometric combination of K_3GV-PDA and D_3GV-PDA in the coassembled sample. Relative to the K_3GV-PDA sample, we obtained intensities between 0.60 and 0.70 for the D_3GV-PDA and coassembly samples. The observations of relatively wide peak linewidths, longer required ultracentrifugation times, and lower peak intensities for the D_3GV-PDA and coassembly samples indicate that they did not assemble as well as the K_3GV-PDA sample. Collectively, these structural characterizations confirm the formation of 1-D nanostructures for the single- and two-component samples, as well as the relative assembly order adapted by the peptide moiety under the polymerization conditions used for DA monomers.

Structure-Dependent Photophysical Properties of Peptide-PDA Conjugates under Ambient Conditions. Incorporating peptides as an appendage to the alkyl-DA is expected to impact the resulting chromatic phase after the photopolymerization based on how they influence the initial assembly order or degree of monomer packing. Similarly, for these amphiphilic monomers, any structural changes in the peptide region are expected to simultaneously impact the PDA conformation and the resulting photophysical properties. In PDA systems, the changes in the π-electron delocalization length of the ene-yne conjugated backbone contribute to the blue and red phases. The induced torsion in the ene-yne conjugated backbone is suggested to influence the effective π-conjugation length, to broaden the energy gap, and to enhance the vibration amplitude of the bonds in the backbone as the system transitions from blue-to-red.[41,42] In this section, we describe the absorbance profiles and assembly behavior of samples that were polymerized under neutral pH and ambient conditions (Figure 3). At room temperature, both charged single-component peptide-PDAs (K_3GV-PDA and D_3GV-PDA) show absorption peaks which suggest the coexistence of both the planar blue PDA phase (λ_{max} ~630 nm) and the twisted red PDA phase (λ_{max} ~540 nm), with the latter being the more predominant peak (Figure 3b). Additionally, the single-component samples have a noticeable ~570 nm peak that can be attributed to a "purple" phase as either a distinct kinetic intermediate between the blue-to-red transition or the presence of multiple electronic structures according to previous literature reports.[43,44] The more ordered K_3GV-PDA self-assembled structures in solution showed a lower red/blue peak intensity ratio than D_3GV-PDA (Table S2). For the two-component sample, where there is the electrostatic interaction between the oppositely charged monomers in addition to the expected noncovalent interactions between peptides, the red/blue peak intensity ratio is much higher than the single-component samples and the purple phase peak is not as distinct, suggesting that the electrostatic interactions provide stabilizing interactions that favor the formation of the more twisted red phase (Table S2).

We also examined the CD spectra of the peptide-polymer conjugates, whereby the peaks in the 190−260 nm region for K_3GV-PDA and the equimolar coassembled samples exhibit signals that suggest β-sheet-like secondary structures (Figure 3c). On the other hand, D_3GV-PDA alone demonstrated CD signals reminiscent of random coils. These observations were consistent with the relative order of all three samples deduced from the ssNMR studies. To provide complementary structural information to CD data, we performed ATR-FTIR characterization on lyophilized peptide-PDA samples (i.e., from room-temperature solutions and those that underwent a heating-cooling treatment cycle; Figure S13 and Table S3). We note that the PDA C═C stretching bands overlap within the amide I/II region. Among the three samples, the K_3GV-PDA samples show the most prominent spectral signatures reminiscent of β-sheet-like structures, particularly with the peak shoulder at ~1680 cm^{-1} representing one of the β-sheet amide I bands. These data are consistent with the results of ssNMR and CD, indicating that K_3GV-PDA has a higher degree of structural order than the coassembled sample and D_3GV-PDA. Interestingly, a new peak around ~1577 cm^{-1} was also observed in both the untreated and thermally treated coassembled sample, further supporting that the two-component sample is coassembled and is interacting with each other in a way that creates a distinct assembly environment from the one-component assemblies. Altogether, the comprehensive characterization data presented herein establishes the relative degrees of assembly order for the one-component and coassembled peptide-PDAs studied here that all form 1-D nanostructures under pH-neutral, aqueous conditions.

As a control experiment to further assess how the electrostatic interactions impact the polymerization in the two-component assembly, we prepared D_3GV appended to a bare alkyl chain using PA (PA; forming D_3GV-PA). D_3GV-PA was coassembled with K_3GV-DA, where the total molar concentrations of the peptide components were kept the same as the single-component solutions. Ideally, for the DA monomers to become PDAs, they must meet the geometric requirements for DA topochemical polymerization, such as achieving ~5 Å distance.[10] Thus, if the peptide-DA monomers are self-sorting [Figure 3a(i)] and the additional electrostatic interactions only cause further lateral bundling rather than 1-D growth of the assemblies prior to photopolymerization, then the absorbance peaks and the corresponding area under the curve should be half of when the two peptides are bearing DA units. If a perfect alternating supramolecular polymer is formed [Figure 3a(iii)], then the DA monomers from K_3GV-DA will be completely blocked from polymerization due to the inability to meet the geometric requirements mentioned above. Figure 3d shows that neither of these two scenarios is likely the case since polymerization still occurred, but the peaks are less than half the intensity/area of the K_3GV-PDA/D_3GV-PDA sample. Thus, the absorbance profile of the K_3GV-PDA/D_3GV-PA coassembly suggests that blocks of K_3GV-PDA are more likely to be polymerized within a longer coassembled chain with D_3GV-PA [Figure 3a(ii)] rather than achieving a self-sorted scenario [Figure 3a(i)] or a perfectly alternating supramolecular coassembly along the long axis [Figure 3a(iii)]. Additionally, the CD spectra in Figure 3e confirm that the secondary structure adapted by the samples used for this control experiment also shows a β-sheet spectral signature similar to that shown in Figure 3c. Formation of the 1-D nanostructure for their polymerized K_3GV-PDA/D_3GV-PDA and K_3GV-PDA/D_3GV-PA samples was visualized using TEM (Figure 3f,g). These experiments confirm that our coassembly is unlikely to be dominated by self-sorted K_3GV-PDA and D_3GV-PDA nanostructures that are bundling laterally due to electrostatic interactions. Instead, our data suggest that our coassembly is more likely to have both

https://doi.org/10.1021/acs.biomac.3c00422
Biomacromolecules 2023, 24, 4051−4063

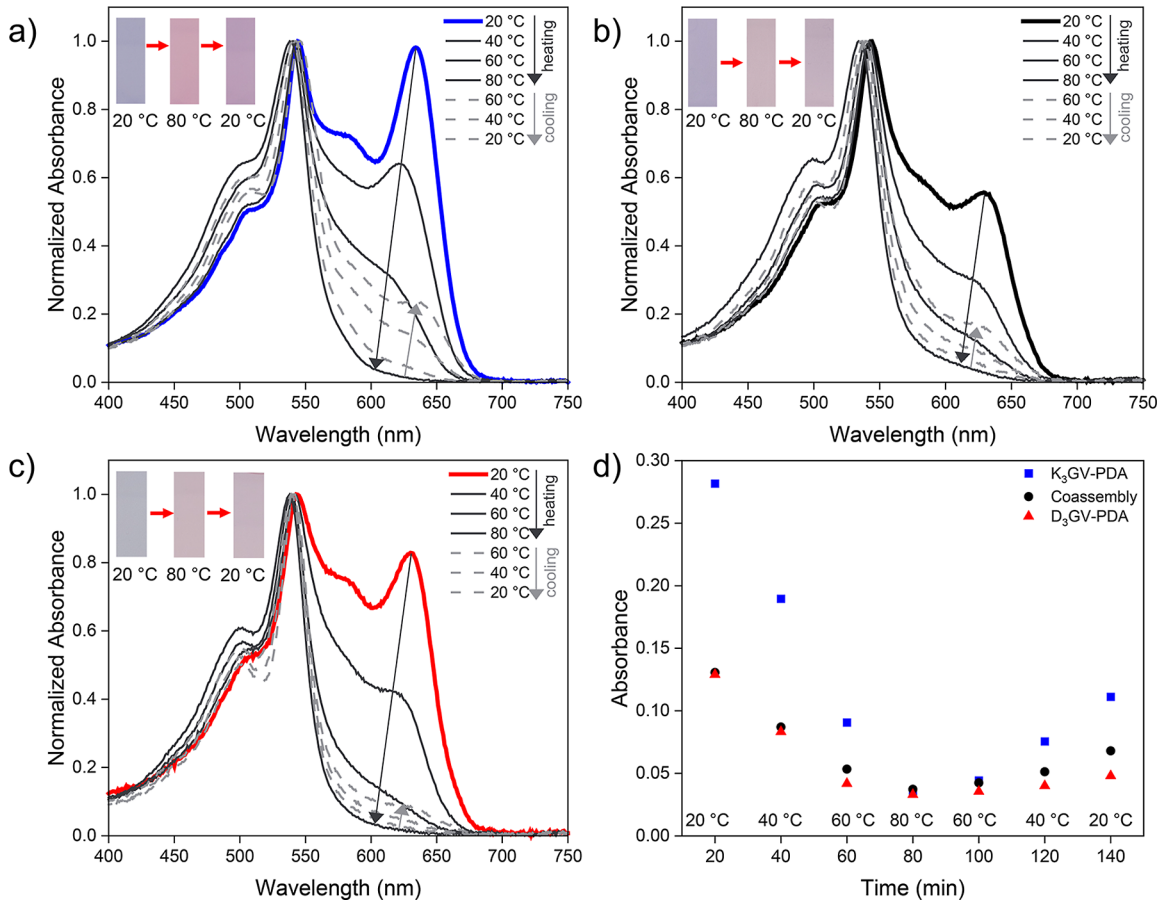

Figure 4. Solution-phase peptide-PDA thermochromism. Evolution of absorbance profiles of 0.66 mM peptide-PDA solutions during the heating-cooling cycle: (a) K_3GV-PDA; (b) 1:1 coassembly; and (c) D_3GV-PDA; solid lines represent heating cycles and dashed lines represent cooling cycles. The rate of temperature change was set at 4 °C/min. (d) Recovery of λ_{630nm} at each temperature.

peptides, K_3GV and D_3GV, in the same PDA-conjugated chains upon polymerization.

Thermochromic Response of Charged Peptide-PDAs in Aqueous Conditions. In the previous sections, we showed the peptide-PDA absorption profiles under ambient conditions and systematically established the structure and assembly behavior of the charged peptide-PDAs and their equimolar coassembly. With the precedence of thermochromicity in PDA and PDA-based assemblies, we investigated how the photophysical properties of these peptide-polymer conjugates, particularly their absorbance and CD spectra, evolve in response to changes in temperature. The variation in the peptide moieties between the charged, single-component samples and their coassembly was assessed on how it influences the PDA thermochromicity during a stepwise heating period from 20 to 80 °C and cooling back to 20 °C (Figures 4 and S14 and Table S4). Based on the normalized absorbance spectra with respect to the λ_{max} (~540 nm) corresponding to the PDA red phase, for all three conditions, the intensity ratio of the blue phase λ_{max} (~630 nm) to the red phase peak decreases as the temperature increases from 20 to 80 °C. At 80 °C, the peak corresponding to the PDA blue phase is completely diminished for all three conditions. We also observed the hypsochromic shifts of the peaks corresponding to the PDA red phase around ~540 nm as temperature changes. These changes are consistent with previous literature reports about these two phases, whereby the PDA red phase represents the electronic structure of a PDA-conjugated backbone that is more twisted than the PDA blue phase.[13,22] To quantify the spectral evolution in response to temperature changes in the blue phase, we calculated the CR of each sample based on the corresponding peaks for the PDA red and blue phases at 20 °C before and after the full heating cycle. The highest CR and lowest peak reversibility were observed for the less ordered D_3GV-PDA with 61.4% (closer to 100% means less reversible), while that of K_3GV-PDA and the coassembled samples have CR equal to 53.1 and 43.3%, respectively. When interpreting these data, we consider the interactions that are at play as the temperature increases (or decreases) and how the charged peptidic moieties influence the PDA conformation that is responsible for the chromatic transitions. The temperature-dependent absorbance spectra, therefore, suggest that the electrostatic interactions between the K_3GV-PDA and D_3GV-PDA moieties in coassembled samples serve as an additional templating interaction during the heating and cooling processes. Our results suggest that the electrostatic templating renders the PDA backbone less susceptible to conformational hysteresis in the solution state as compared to the D_3GV-PDA and K_3GV-PDA alone.

To better understand the structural changes that accompany the chromatic transitions during temperature changes, we also monitored the 190−260 nm region of the CD spectra of samples within the temperature range of interest (Figure 5). At a rate of 4 °C/min, K_3GV-PDA consistently exhibited CD peaks reminiscent of a β-sheet structure until 60 °C. When the temperature was further increased to 80 °C, the intensity of the CD peaks decreased. D_3GV-PDA showed CD spectral features reminis-

https://doi.org/10.1021/acs.biomac.3c00422
Biomacromolecules 2023, 24, 4051−4063

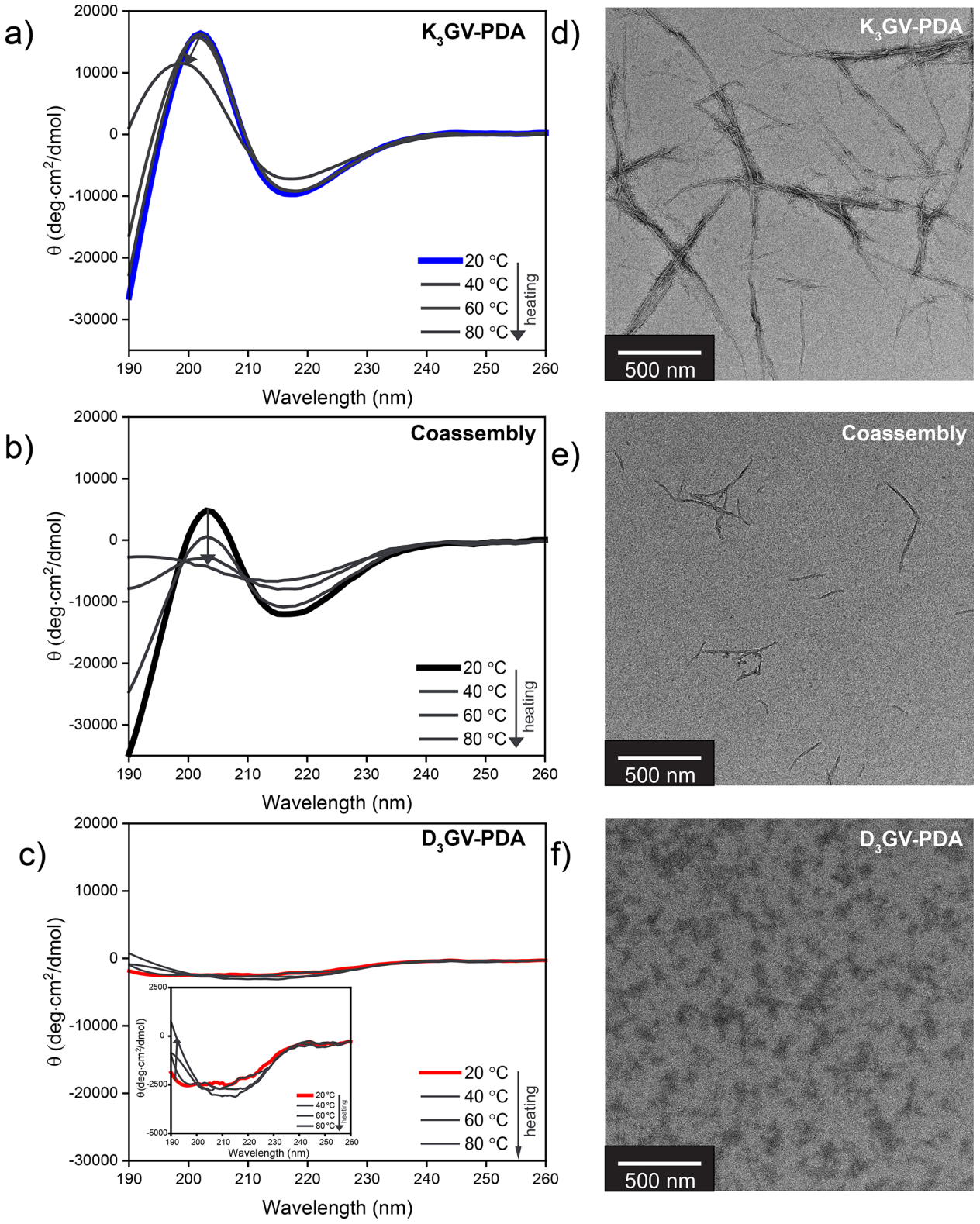

Figure 5. Distinct structural features of peptide-PDA nanostructures in response to changes in temperature. (a−c) Evolution of CD spectra in response to increasing temperature changes (20−80 °C, 4 °C/min) for all three samples. Inset (in c): CD spectra for D_3GV-PDA. (d−f) Representative TEM images peptide-PDA nanostructures heated and then instantaneously cooled to room temperature. All three samples (0.66 mM, pH 7) were polymerized at room temperature, and temperature was maintained throughout measurements. Scale bar = 500 nm.

cent of random coils at all temperatures. These structural observations can also be attributed to the lower charge repulsion expected for K_3GV-PDA than D_3GV-PDA arising from the positively charged side chain of lysine which is more flexible and longer compared to the negatively charged side chain of aspartic acid. From this, it can be concluded that the charge repulsion from triaspartic acids in neutral pH prevented the peptides to form stable aggregates upon heating. Interestingly, the CD

https://doi.org/10.1021/acs.biomac.3c00422
Biomacromolecules 2023, 24, 4051−4063

spectra for the two-component coassembly show that the secondary structure of the mixture transitioned from β-sheet to random coil as the temperature increased, and the secondary structure was disrupted when it was exposed to 80 °C. The resulting secondary structures of the coassembly can be rationalized by the electrostatic interactions programmed through the peptidic backbone, which helps the coassembly to exist as a stable structure in the aqueous environment in addition to the other non-covalent interactions intrinsic to the peptide-PDA building blocks. The K_3GV-PDA and the coassembled peptide-PDAs maintained nanostructures with 1-D morphologies after heating to 80 °C and cooling back to room temperature, whereas D_3GV-PDA started to show polymer aggregates with a more random morphology after going through this heat-cool process (Figure 5d−f).

Thermochromic Response of Charged Peptide-PDAs Films. Beyond electronic transitions and structural evolution in the solution phase, we also studied the peptide-directed conformational changes in the conjugated backbone that lead to the chromogenic transitions of peptide-PDA drop-casted films using micro-Raman spectroscopy (Figures 6 and S15−S18). The Raman peaks that correspond to the ene-yne conjugated backbone of PDAs at ∼1500 cm^{-1} (C═C) and ∼2100 cm^{-1} (C≡C) were used to track the dominance of the blue (∼1450 and ∼2080 cm^{-1})[13,45] or the red phase (∼1500 and ∼2100 cm^{-1})[45,46] under various temperature points that we tested herein. As PDA transitions from the blue to red phase, the side-chain arrangement is less restricted, resulting in a greater vibration amplitude of the C═C bonds. As a result, the bond vibration of the C═C bond scatters at a higher energy, and the Raman peaks shift to a larger wavenumber.[42] Based on the absorbance spectra in Figure 3, we know that the two dominant peaks at ∼540 and ∼630 nm can be primarily excited to produce a strongly enhanced resonance Raman signal when 532 and 633 nm laser sources are used for excitation. The resulting Raman spectra from exciting at various laser wavelengths (473, 532, 633, and 785 nm; Figure S15) confirm that 633 nm is the optimal excitation source to use for monitoring the existence of blue phase species at different temperatures under ambient conditions. On the other hand, 532 nm can be used to monitor the red phase PDA for single-component samples and their coassembly. The temperature-dependent Raman spectra of the three peptide-PDA films excited at 633 nm provide evidence for the transition of chains that are initially in the blue phase to the red phase (Figure 6a,b,e,f,i,j) through the appearance of ∼1500 and ∼2100 cm^{-1} bands. The peaks in the 1000−1150 cm^{-1} region (∼1080, 1110, and 1130 cm^{-1}) have modes associated with C−C rotations (in the PDA backbone) and vibrational modes related to side-chain groups. The temperature-dependent changes in these spectra suggest conformational changes occurring in these structures (Figure S16). The weakening of bands in the 1000−1150 cm^{-1} region is reminiscent of alkyl chains adjacent to PDAs that are more in the red phase than in the blue phase. There is also a big peak shift of the ∼1080 cm^{-1} mode in the coassembled sample that can be attributed to the conformation change. In addition, the coassembled sample excited at 633 nm has a larger shift and a lower energy mode than both of the single-component samples in this region (Figure S16).

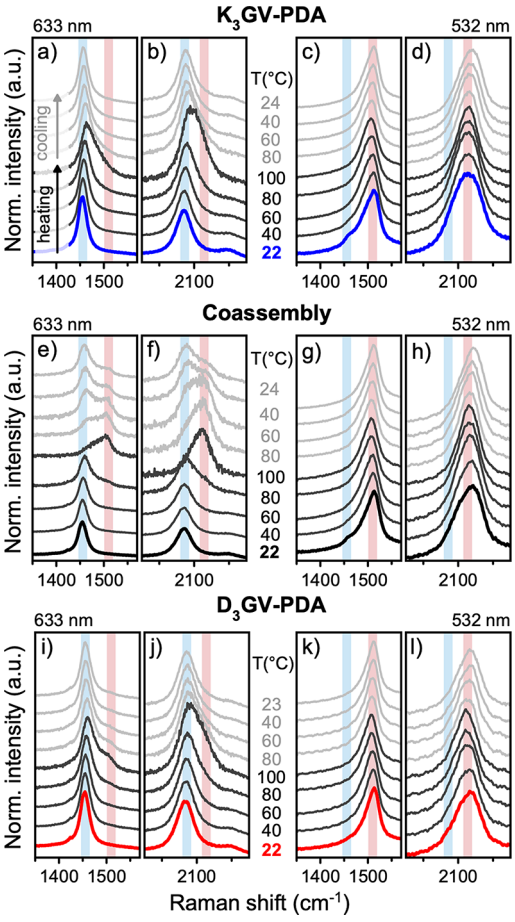

Figure 6. Thermochromic behavior of peptide-PDA films using Raman spectroscopy. The peak evolution of (a−d) K_3GV-PDA, (e−h) coassembled sample, and (i−l) D_3GV-PDA samples is measured for C═C (∼1500 cm^{-1}) and C≡C (∼2100 cm^{-1}) at 532 and 633 nm. Black curves represent heating cycles and gray lines represent cooling cycles, as represented by the arrows in (a). The heating and cooling rate for samples was 10 °C/min. The regions highlighted in blue and red correspond to the inherent blue phase and red phase presented in the peptide-PDA system.

Comparing Figure 6a,b,e,f,i,j excited at 633 nm, the highest degree of blue-to-red transition is facilitated by the coassembled sample where the red phase peaks ∼1500 and ∼2100 cm^{-1} are observed starting at 80 °C. For both the K_3GV- and D_3GV-PDA films, peak broadening that suggests the development of red phase peaks also starts to become evident at 80 °C. Upon cooling down the single-component polymer samples to the initial temperature (23∼24 °C), the red phase peaks disappear, and the blue phase peak intensities recover only about 30−40% of the initial values. Similarly, the coassembled sample recovered ∼5−6% of its original intensity, significantly less than the single-component samples, indicating a non-reversible thermochromic behavior for our model peptides and their coassembly. The evolution of blue-to-red transitions of the K_3GV-PDA, D_3GV-PDA, and their coassembled sample is quantified at each temperature (Figure S17). Compared to each single-component sample, there was a higher observed red-to-blue ratio that is associated with the coassembled sample in both C═C and C≡C regions, indicating a synergistic effect from the bonding environment that promotes the formation of a less ordered phase. These results suggest that the side-chain interactions facilitated within the coassembled sample stabilize the formation of the twisted red phase at higher temperatures and during the cooling process.

https://doi.org/10.1021/acs.biomac.3c00422
Biomacromolecules 2023, 24, 4051−4063

In addition to the temperature-dependent evolution of the peak profiles and intensities that provided insights into the dynamics of the blue-to-red phase transformation, the shifts in the peak position further provided evidence of the distinct structural changes arising from the phase transition. The peak position of the blue phase for all three samples increased to a maximum value at 100 °C and eventually returned to within 3−5 cm^{-1} of its original value when cooled to room temperature (Figure 6a,b,e,f,i,j). The largest Raman shift change is observed in the coassembled sample, with an increase of 25 cm^{-1} (C═C region) and 15 cm^{-1} (C≡C region), which is 2−3 times larger compared to the individual components (Figure S18). This stark contrast in the peak position points to the conclusion that the coassembled sample experiences the largest increase in the nonplanarity of the polymer backbone of the blue phase. The peak position of the red phase shows a decreasing trend with temperature with the same rate in peak position change, suggesting that this is most likely associated with the inherent temperature-dependent behavior and not due to the disorder (Figure 6c,d,g,h,k,l).[47] In addition, the RGB analysis of the films during the temperature-dependent studies suggests that the peptide-PDA samples become more red with the increasing temperature, and the amount of the blue component remains relatively unchanged across the different temperatures (Figure S19). Overall, the Raman spectra of the film samples underscore the impact of varied non-covalent side-chain interactions on the chromatic phases adapted by the PDAs at various temperatures, whereby attractive electrostatic interactions present in the coassembled phase support a greater degree of torsion for PDA films during temperature variation. However, similar to the solution phase samples shown in Figure 4, these interactions did not contribute to promoting reversibility in thermochromism for the solid-phase samples in Figure 6, likely due to the emergent electrostatic interactions that were found here to be stabilizing the red PDA phase.

CONCLUSIONS

In summary, this work provides insights into how charged H-bonding moieties can be used to modulate the structural states responsible for the thermochromic transitions of amphiphilic PDAs. We used charged pentapeptides (K_3GV and D_3GV) as the polar side chain of an amphiphilic DA monomer, as well as their coassemblies, to be our model system for this work. Charged peptide moieties and their coassembly afford the geometric requirements necessary to facilitate the topochemical polymerization of peptide-DAs. The peptide-PDAs (K_3GV-PDA and D_3GV-PDA) and their coassemblies with varying order and 1-D nanostructure lengths were investigated for their thermochromic behavior in solution and film state under pH 7. In particular, pure K_3GV-PDA forms β-sheet like assemblies that are more ordered than pure D_3GV-PDA, which adopt a secondary structure reminiscent of random coils. Through the photophysical and structural characterizations performed on the single- and two-component samples in solution and film state, this work represents the first study to map out the structural/conformational transformations associated with the thermochromicity of chromogenic polymers processed under aqueous conditions as mediated by charged, H-bonding side chains. We learned that the additional attractive electrostatic interactions among the peptidic side chains of PDA act to stabilize the red phase more than the blue phase. This paper demonstrates how the manipulation of electrostatic interactions through bio-inspired side-chain engineering of chromogenic polymers offers a broad range of synthetic handles for precisely controlling the dynamic and stimuli-responsive properties, such as thermochromicity, of adaptive π-conjugated polymeric materials.

ASSOCIATED CONTENT

Supporting Information

The Supporting Information is available free of charge at https://pubs.acs.org/doi/10.1021/acs.biomac.3c00422.

Characterization of peptide-DA and peptide-PDA samples (NMR, ESI-MS, HPLC, and GPC) and additional absorbance, FTIR, and Raman spectroscopy data on thermally treated samples (PDF)

AUTHOR INFORMATION

Corresponding Author

Herdeline Ann M. Ardoña − *Department of Chemical and Biomolecular Engineering, Samueli School of Engineering, Department of Chemistry, School of Physical Sciences, Department of Biomedical Engineering, Samueli School of Engineering, and Sue & Bill Gross Stem Cell Research Center, University of California, Irvine, California 92697, United States;* orcid.org/0000-0003-0640-1262; Email: hardona@uci.edu

Authors

Sujeung Lim − *Department of Chemical and Biomolecular Engineering, Samueli School of Engineering, University of California, Irvine, California 92697, United States*

Dmitri Leo M. Cordova − *Department of Chemistry, School of Physical Sciences, University of California, Irvine, California 92697, United States*

Alicia S. Robang − *School of Chemical and Biomolecular Engineering, Georgia Institute of Technology, Atlanta, Georgia 30332, United States*

Yuyao Kuang − *Department of Chemical and Biomolecular Engineering, Samueli School of Engineering, University of California, Irvine, California 92697, United States*

Kaleolani S. Ogura − *Department of Chemistry, School of Physical Sciences, University of California, Irvine, California 92697, United States*

Anant K. Paravastu − *School of Chemical and Biomolecular Engineering, Georgia Institute of Technology, Atlanta, Georgia 30332, United States;* orcid.org/0000-0001-7183-1942

Maxx Q. Arguilla − *Department of Chemistry, School of Physical Sciences, University of California, Irvine, California 92697, United States;* orcid.org/0000-0001-9948-0814

Complete contact information is available at: https://pubs.acs.org/10.1021/acs.biomac.3c00422

Author Contributions

The authors listed above have all substantially contributed to this research article and have approved the final version of the manuscript.

Notes

The authors declare no competing financial interest.

ACKNOWLEDGMENTS

This work was supported by startup funds from the University of California, Irvine (UCI) and was partially supported by the National Science Foundation (DMR-2239647 to H. A. M. A. and OAC-1931430 to A. K. P.). The authors acknowledge the use of facilities and instrumentation at the UC Irvine Materials

Research Institute (IMRI), which is also supported in part by the National Science Foundation Materials Research Science and Engineering Center: Center for Complex and Active Materials (DMR-2011967). In addition, ssNMR spectra were collected at the Georgia Tech NMR Center. The authors thank the Horiba Institute for Mobility and Connectivity^2 (HIMaC^2) for the use of their Horiba Raman spectrometer. The authors also thank Dr. Dmitry Fishman for the access to equipment in the Laser Spectroscopy Laboratories, as well as Ricardo De Luna at the UCSD Materials Research Science and Engineering Center for the GPC characterization. The authors thank Dr. Zefan Yao as well for providing assistance on the GPC data analysis.

REFERENCES

(1) Weston, M.; Kuchel, R. P.; Chandrawati, R. A.-O. A Polydiacetylene-Based Colorimetric Sensor as an Active Use-By Date for Plant-Based Milk Alternatives. *Macromol. Rapid Commun.* **2020**, *41*, 2000172.

(2) Wang, M.; Wang, F.; Wang, Y.; Zhang, W.; Chen, X. Polydiacetylene-based sensor for highly sensitive and selective Pb^{2+} detection. *Dyes Pigm.* **2015**, *120*, 307−313.

(3) Lee, C. G.; Kang, S.; Oh, J.; Eom, M. S.; Oh, J.; Kim, M.-G.; Lee, W. S.; Hong, S.; Han, M. S. A colorimetric and fluorescent chemosensor for detection of Hg^{2+} using counterion exchange of cationic polydiacetylene. *Tetrahedron Lett.* **2017**, *58*, 4340−4343.

(4) Eaidkong, T.; Mungkarndee, R.; Phollookin, C.; Tumcharern, G.; Sukwattanasinitt, M.; Wacharasindhu, S. Polydiacetylene paper-based colorimetric sensor array for vapor phase detection and identification of volatile organic compounds. *J. Mater. Chem.* **2012**, *22*, 5970−5977.

(5) Phonchai, N.; Khanantong, C.; Kielar, F.; Traiphol, R.; Traiphol, N. Low-Temperature Reversible Thermochromic Polydiacetylene/Zinc(II)/Zinc Oxide Nanocomposites for Colorimetric Sensing. *ACS Appl. Nano Mater.* **2019**, *2*, 4489−4498.

(6) Chen, X.; Yoon, J. A thermally reversible temperature sensor based on polydiacetylene: Synthesis and thermochromic properties. *Dyes Pigm.* **2011**, *89*, 194−198.

(7) Huo, J.; Hu, Z.; He, G.; Hong, X.; Yang, Z.; Luo, S.; Ye, X.; Li, Y.; Zhang, Y.; Zhang, M.; Chen, H.; Fan, T.; Zhang, Y.; Xiong, B.; Wang, Z.; Zhu, Z.; Chen, D. High temperature thermochromic polydiacetylenes: Design and colorimetric properties. *Appl. Surf. Sci.* **2017**, *423*, 951−956.

(8) Park, I. S.; Park, H. J.; Kim, J. M. A soluble, low-temperature thermochromic and chemically reactive polydiacetylene. *ACS Appl. Mater. Interfaces* **2013**, *5*, 8805−8812.

(9) Fang, F.; Meng, F.; Luo, L. Recent advances on polydiacetylene-based smart materials for biomedical applications. *Mater. Chem. Front.* **2020**, *4*, 1089−1104.

(10) Qian, X.; Städler, B. Recent Developments in Polydiacetylene-Based Sensors. *Chem. Mater.* **2019**, *31*, 1196−1222.

(11) Joung, J. F.; Baek, J.; Kim, Y.; Lee, S.; Kim, M. H.; Yoon, J.; Park, S. Electronic relaxation dynamics of PCDA-PDA studied by transient absorption spectroscopy. *Phys. Chem. Chem. Phys.* **2016**, *18*, 23096−23104.

(12) Huo, J.; Deng, Q.; Fan, T.; He, G.; Hu, X.; Hong, X.; Chen, H.; Luo, S.; Wang, Z.; Chen, D. Advances in polydiacetylene development for the design of side chain groups in smart material applications − a mini review. *Polym. Chem.* **2017**, *8*, 7438−7445.

(13) Filhol, J.-S.; Deschamps, J.; Dutremez, S. G.; Boury, B.; Barisien, T.; Legrand, L.; Schott, M. Polymorphs and Colors of Polydiacetylenes: A First Principles Study. *J. Am. Chem. Soc.* **2009**, *131*, 6976−6988.

(14) Chu, B.; Xu, R. Chromatic transition of polydiacetylene in solution. *Acc. Chem. Res.* **1991**, *24*, 384−389.

(15) Oikawa, H.; Korenaga, T.; Okada, S.; Nakanishi, H. Chromatic transition of π-conjugated polydiacetylene and the subsequent aggregation phenomena. *Polymer* **1999**, *40*, 5993−6001.

(16) Weston, M.; Tjandra, A. D.; Chandrawati, R. Tuning chromatic response, sensitivity, and specificity of polydiacetylene-based sensors. *Polym. Chem.* **2020**, *11*, 166−183.

(17) Yu, L.; Hsu, S. L. A Spectroscopic Analysis of the Role of Side Chains in Controlling Thermochromic Transitions in Polydiacetylenes. *Macromolecules* **2012**, *45*, 420−429.

(18) Huang, Q.; Wu, W.; Ai, K.; Liu, J. Highly Sensitive Polydiacetylene Ensembles for Biosensing and Bioimaging. *Front. Chem.* **2020**, *8*, 565782.

(19) Zhu, L.; Tran, H.; Beyer, F. L.; Walck, S. D.; Li, X.; Ågren, H.; Killops, K. L.; Campos, L. M. Engineering Topochemical Polymerizations Using Block Copolymer Templates. *J. Am. Chem. Soc.* **2014**, *136*, 13381−13387.

(20) Kuang, Y.; Yao, Z.-F.; Lim, S.; Ngo, C.; Rocha, M. A.; Fishman, D. A.; Ardoña, H. A. M. Biomimetic Sequence-Templating Approach toward a Multiscale Modulation of Chromogenic Polymer Properties. *Macromolecules* **2023**, *56*, 4526−4540.

(21) Yoon, B.; Shin, H.; Kang, E.-M.; Cho, D. W.; Shin, K.; Chung, H.; Lee, C. W.; Kim, J.-M. Inkjet-Compatible Single-Component Polydiacetylene Precursors for Thermochromic Paper Sensors. *ACS Appl. Mater. Interfaces* **2013**, *5*, 4527−4535.

(22) Mergu, N.; Son, Y.-A. Design and synthesis of polydiacetylenes, and their low temperature irreversible thermochromic properties. *Dyes Pigm.* **2021**, *184*, 108839.

(23) Koga, T.; Taguchi, T.; Higashi, N. β-Sheet peptide-assisted polymerization of diacetylene at the air−water interface and thermochromic property. *Polym. J.* **2012**, *44*, 195−199.

(24) Palladino, P.; Castelletto, V.; Dehsorkhi, A.; Stetsenko, D.; Hamley, I. W. Reversible thermal transition of polydiacetylene based on KTTKS collagen sequence. *Chem. Commun.* **2012**, *48*, 9774−9776.

(25) Guo, H.; Zhang, J.; Porter, D.; Peng, H.; Löwik, D. W. P. M.; Wang, Y.; Zhang, Z.; Chen, X.; Shao, Z. Ultrafast and reversible thermochromism of a conjugated polymer material based on the assembly of peptide amphiphiles. *Chem. Sci.* **2014**, *5*, 4189−4195.

(26) Pires, A. C.; Soares, N. d. F. F.; da Silva, L. H. M.; da Silva, M. C. H.; Mageste, A. B.; Soares, R. F.; Teixeira, Á. V. N. C.; Andrade, N. J. Thermodynamic study of colorimetric transitions in polydiacetylene vesicles induced by the solvent effect. *J. Phys. Chem. B* **2010**, *114*, 13365−13371.

(27) Jeon, S.; Yoon, B.; Kim, J.-M. Polymerization Temperature-dependent Thermochromism of Polydiacetylene. *Bull. Korean Chem. Soc.* **2015**, *36*, 1949−1950.

(28) White, A. D.; Keefe, A. J.; Ella-Menye, J.-R.; Nowinski, A. K.; Shao, Q.; Pfaendtner, J.; Jiang, S. Free Energy of Solvated Salt Bridges: A Simulation and Experimental Study. *J. Phys. Chem. B* **2013**, *117*, 7254−7259.

(29) Zhou, H.-X.; Pang, X. Electrostatic Interactions in Protein Structure, Folding, Binding, and Condensation. *Chem. Rev.* **2018**, *118*, 1691−1741.

(30) Klimov, D. K.; Thirumalai, D. Dissecting the Assembly of Aβ16−22 Amyloid Peptides into Antiparallel β Sheets. *Structure* **2003**, *11*, 295−307.

(31) Hamsici, S.; White, A. D.; Acar, H. Peptide framework for screening the effects of amino acids on assembly. *Sci. Adv.* **2022**, *8*, No. eabj0305.

(32) Hu, Y.; Lin, R.; Zhang, P.; Fern, J.; Cheetham, A. G.; Patel, K.; Schulman, R.; Kan, C.; Cui, H. Electrostatic-Driven Lamination and Untwisting of β-Sheet Assemblies. *ACS Nano* **2016**, *10*, 880−888.

(33) Cui, H.; Cheetham, A. G.; Pashuck, E. T.; Stupp, S. I. Amino Acid Sequence in Constitutionally Isomeric Tetrapeptide Amphiphiles Dictates Architecture of One-Dimensional Nanostructures. *J. Am. Chem. Soc.* **2014**, *136*, 12461−12468.

(34) Yao, Z.-F.; Kuang, Y.; Kohl, P.; Li, Y.; Ardoña, H. A. M. Carbodiimide-Fueled Assembly of π-Conjugated Peptides Regulated by Electrostatic Interactions. *ChemSystemsChem* **2023**, *5*, No. e202300003.

(35) Nieuwland, M.; van Gijzel, N.; van Hest, J. C. M.; Löwik, D. W. P. M. The influence of amino acid sequence on structure and morphology of polydiacetylene containing peptide fibres. *Soft Matter* **2015**, *11*, 1335−1344.

(36) Ahmed, S.; Pramanik, B.; Sankar, K. N. A.; Srivastava, A.; Singha, N.; Dowari, P.; Srivastava, A.; Mohanta, K.; Debnath, A.; Das, D.

https://doi.org/10.1021/acs.biomac.3c00422
Biomacromolecules 2023, 24, 4051−4063

Solvent Assisted Tuning of Morphology of a Peptide-Perylenediimide Conjugate: Helical Fibers to Nano-Rings and their Differential Semiconductivity. *Sci. Rep.* **2017**, *7*, 9485.
(37) Romero, P. R.; Kobayashi, N.; Wedell, J. R.; Baskaran, K.; Iwata, T.; Yokochi, M.; Maziuk, D.; Yao, H.; Fujiwara, T.; Kurusu, G.; Ulrich, E. L.; Hoch, J. C.; Markley, J. L. BioMagResBank (BMRB) as a Resource for Structural Biology. *Methods in Molecular Biology*; Gáspári, Z., Ed.; Humana: New York, NY, 2020; Vol. *2112*, pp 187−218.
(38) Nava, A. D.; Thakur, M.; Tonelli, A. E. Carbon-13 NMR structural studies of a soluble polydiacetylene, poly(4BCMU). *Macromolecules* **1990**, *23*, 3055−3063.
(39) Colvin, M. T.; Silvers, R.; Frohm, B.; Su, Y.; Linse, S.; Griffin, R. G. High Resolution Structural Characterization of Aβ_{42} Amyloid Fibrils by Magic Angle Spinning NMR. *J. Am. Chem. Soc.* **2015**, *137*, 7509−7518.
(40) Dong, H.; Paramonov, S. E.; Aulisa, L.; Bakota, E. L.; Hartgerink, J. D. Self-Assembly of Multidomain Peptides: Balancing Molecular Frustration Controls Conformation and Nanostructure. *J. Am. Chem. Soc.* **2007**, *129*, 12468−12472.
(41) Nuck, J.; Sugihara, K. Mechanism of Polydiacetylene Blue-to-Red Transformation Induced by Antimicrobial Peptides. *Macromolecules* **2020**, *53*, 6469−6475.
(42) Wang, Y.; Pei, H.; Jia, Y.; Liu, J.; Li, Z.; Ai, K.; Lu, Z.; Lu, L. Synergistic Tailoring of Electrostatic and Hydrophobic Interactions for Rapid and Specific Recognition of Lysophosphatidic Acid, an Early-Stage Ovarian Cancer Biomarker. *J. Am. Chem. Soc.* **2017**, *139*, 11616−11621.
(43) Carpick, R. W.; Mayer, T. M.; Sasaki, D. Y.; Burns, A. R. Spectroscopic Ellipsometry and Fluorescence Study of Thermochromism in an Ultrathin Poly(diacetylene) Film: Reversibility and Transition Kinetics. *Langmuir* **2000**, *16*, 4639−4647.
(44) Dautel, O. J.; Robitzer, M.; Lère-Porte, J.-P.; Serein-Spirau, F.; Moreau, J. J. E. Self-Organized Ureido Substituted Diacetylenic Organogel. Photopolymerization of One-Dimensional Supramolecular Assemblies to Give Conjugated Nanofibers. *J. Am. Chem. Soc.* **2006**, *128*, 16213−16223.
(45) Exarhos, G. J.; Risen, W. M., Jr.; Baughman, R. H. Resonance Raman study of the thermochromic phase transition of a polydiacetylene. *J. Am. Chem. Soc.* **1976**, *98*, 481−487.
(46) Campbell, A. J.; Davies, C. K. L.; Batchelder, D. N. Raman shifts due to variations in backbone planarity in a group of polydiacetylenes. *Macromol. Chem. Phys.* **1998**, *199*, 109−112.
(47) Spagnoli, S.; Berrehar, J.; Fave, J.-L.; Schott, M. Temperature dependence of spectroscopic properties of isolated polydiacetylene chains strained by their monomer single crystal matrix. *Chem. Phys.* **2007**, *333*, 254−264.

https://doi.org/10.1021/acs.biomac.3c00422
Biomacromolecules 2023, 24, 4051−4063